# Identification of a Response Amplitude Operator for Ships

Giovanni A. Bonaschi (Eindhoven University of Technology), Olena Filatova (Eindhoven University of Technology), Carlo Mercuri (Eindhoven University of Technology), Adrian Muntean (Eindhoven University of Technology), Mark A. Peletier (Eindhoven University of Technology), Volha Shchetnikava (Eindhoven University of Technology), Eric Siero (Leiden University), Iason Zisis (Eindhoven University of Technology)

### Abstract

At the European Study Group Mathematics with Industry 2012 in Eindhoven, the Maritime Research Institute Netherlands (MARIN) presented the problem of identifying the response amplitude operator (RAO) for a ship, given input information on the amplitudes of the sea waves and output information on the movement of the ship. We approach the problem from a threefold perspective: a direct least-squares approach, an approach based on truncated Fourier series, and an approach using low-dimensional measures of the RAO. We give a few recommendations for possible further investigations.

KEYWORDS: Parameter/structure identification, inverse problem, response amplitude operator, ship structure, fatigue estimation

## 1   Introduction

In the present paper we deal with a problem proposed by MARIN during the SWI 2012 workshop in Eindhoven. MARIN, the Maritime Research Institute Netherlands, is an independent service provider for the maritime industry. MARIN's customers include commercial ship builders, fleet owners, navies, naval architects, and offshore companies.

The problem we tackle here is the identification of the structure response amplitude operator (RAO) of a 230m long FPSO, given sets of input-output data, which will be explained in Section 2.

A floating production, storage and offloading (FPSO) unit is a floating vessel used by the offshore industry for the storage and processing of oil and gas, and it is typically moored at a fixed position at sea. The structure is exposed to a natural process of degradation related to the cyclic loading of the structure through time: *fatigue*. This is due to continuously incoming sea waves and wind.

This topic has been studied extensively in the literature according to different points of view; see for example [1, 3, 4] and the references mentioned therein.

The interest of MARIN in the identification of the RAO lies in its use to estimate the expected time until the formation of fatigue cracks. The methods that we discuss in this report might be used to improve the accuracy of numerically calculated RAOs, and lead to a better estimate of the fatigue lifetime. We keep this in mind when discussing the different possible working strategies.

## 2 The data

The data provided by MARIN are generated by two different detection devices.

- A buoy at some distance from the FPSO measures water surface height and angle, and converts these into a wave energy spectrum. For each 30-minute interval indexed by $k$ this results in a discretely defined function $S_\zeta^{(k)}(\omega, \theta)$, which gives the energy contained in waves moving in direction $\theta$ with frequency $\omega$.

- A number of strain gauges on the FPSO measures a local strain in the structure, and converts this into another energy spectrum. This results in a discretely defined function $S_R^{(k)}(\omega, d(k))$, measured at the same time $k$, which gives the energy contained in harmonic bending modes with frequency $\omega$.

- The *draft* $d(k)$ is the vertical distance between the waterline and the bottom of the hull at the time of measurement $k$. This draft changes over time, since the structure accumulates oil and gas over time, and periodically offloads it to transport ships. According to MARIN, the draft has a significant effect on the behaviour of the structure, and this is why this draft is taken into account.

The measurement data is organized as follows.

($\theta$) The measurements of $S_\zeta$ are taken along discretized directions of 4 degrees each (91 in total; $\theta_1 = 0$ and $\theta_{91} = 360$ coincide).

($\omega$) The frequency range for $\omega$ is $0.025 - 0.580$ Hz for $S_\zeta$ and $0 - 0.995$ Hz for $S_R$. For $S_\zeta$ there are 64 different frequencies, 200 for $S_R$. Since the available data for $S_R$ and $S_\zeta$ do not correspond to the same frequency, we convert the values of $S_R$ to the 64-value discretization of $S_\zeta$ by interpolation. As a consequence we do not analyse values of $S_R$ at frequencies greater than $0.58 Hz$ and below $0.025 Hz$.

($d$) The draft of the vessel ranges from 9 to 15 (meters) with $\Delta d = 0.5$, so that there are 12 different drafts.

($k$) Measurements are taken along a period of one year with different draft values as shown in Table 1.

Table 1: Number of measurements for different periods and drafts.

| Draft | July 2007 April 2008 | May 2008 Sept 2008 | Total |
|-------|----------------------|--------------------|-------|
| 9.0-9.5 | 0 | 91 | 91 |
| 9.5-10.0 | 0 | 45 | 45 |
| 10.0-10.5 | 221 | 207 | 428 |
| 10.5-11.0 | 710 | 555 | 1265 |
| 11.0-11.5 | 1482 | 422 | 1904 |
| 11.5-12.0 | 1408 | 464 | 1872 |
| 12.0-12.5 | 893 | 588 | 1481 |
| 12.5-13.0 | 1052 | 124 | 1176 |
| 13.0-13.5 | 902 | 426 | 1328 |
| 13.5-14.0 | 370 | 783 | 1153 |
| 14.0-14.5 | 109 | 202 | 311 |
| 14.5-15.0 | 0 | 92 | 92 |
| Total | 7147 | 3999 | 11146 |

# 3   The mathematical problem

We now describe the mathematical problem that we consider. The response of the FPSO is assumed to follow linear response theory, resulting in the (theoretical) equation (see [1, 2, 3])

$$\forall\, \omega, d: \quad S_R(\omega, d) = \int \Phi_R(\omega, \theta, d) S_\zeta(\omega, \theta)\, d\theta, \tag{1}$$

where, as we described above, $S_R$ and $S_\zeta$ are respectively the total response of the structure and the profile of incoming waves at different angle $\theta$, at a certain frequency $\omega$. $S_R$, $S_\zeta$ and $\Phi_R$ are positive functions; $\Phi_R$ and $S_R$ are assumed to depend also on the draft $d$. The unknown function $\Phi_R$ is, by definition, the response amplitude operator (RAO), and its identification is the aim of this work.

We first convert equation (1) into a discrete, experiment-dependent version:

$$\forall\, \omega, k: \quad S_R^{(k)}(\omega, d(k)) = \sum_\theta \Phi_R(\omega, \theta, d(k))\, S_\zeta^{(k)}(\omega, \theta). \tag{2}$$

We will also reduce to the case of a single draft, using only the 1176 data points corresponding to draft range 12.5–13.0. Therefore we can omit the explicit draft dependence in $S_R$ and $\Phi_R$, and then the equation becomes

$$\forall\, \omega, k: \quad S_R^{(k)}(\omega) = \sum_\theta \Phi_R(\omega, \theta)\, S_\zeta^{(k)}(\omega, \theta). \tag{3}$$

The central question of this paper is therefore:

Can we construct methods for the determination of $\Phi_R$ in (3), given data on $S_R$ and $S_\zeta$?

# 4  Inverse problems and least squares

This problem is a classical inverse problem: determining a physical law from experimental data (see e.g. [6]). For each $\omega$ we need to determine the 91 values of $\Phi_R(\omega, \cdot)$; since for each $\omega$ we have 1176 data points to do so, this is an *a priori* strongly overdetermined problem. The method of first choice in this situation is the least-squares solution.

## Unconstrained least squares

The least-squares method can be interpreted as a method of fitting data. The best fit in the least-square sense is that instance of the model for which the sum of squared residuals has its lowest value, the residual being the difference between an observed value and the value given by the model.

Fix $\omega$, and write $a_{k,j} := S_\zeta^{(k)}(\omega, \theta_j)$, $b_k := S_R^{(k)}$, and $x_j := \Phi_R(\omega, \theta_j)$. Writing $A$ for the matrix of $a_{k,j}$, equation (3) becomes

$$Ax = b \qquad \Longleftrightarrow \qquad \forall k : \sum_j a_{k,j} x_j = b_k. \tag{4}$$

A least-squares solution of (4) is a vector $x$ that minimizes the residual of (4), i.e.

$$x = \arg\min_x \|b - Ax\|_2^2, \tag{5}$$

where $\|\cdot\|_2$ is the standard Euclidean norm.
If $A$ has maximal rank, then this $x$ is given by

$$x = (A^T A)^{-1} A^T b.$$

The MATLAB backslash operator implements this solution concept.

## Constrained least squares

A least-squares solution has no reason to be nonnegative, while the RAO $\Phi_R$ is necessarily nonnegative. The minimization problem (5) has a natural generalization

$$x = \arg\min_{x \geq 0} \|b - Ax\|_2^2,$$

in which $x \geq 0$ should be interpreted as component wise non-negativity. In MATLAB the routine `lsqnonneg` implements this constrained least-squares solution.

# 5   Organization of the report

During the Study Group three different approaches were investigated.

1.  The first approach is to apply the constrained or unconstrained least-squares method directly. In an attempt to reduce the impact of noise, we first made a selection of the most relevant data. This approach is outlined in Section 6.

2.  A second approach used a truncated Fourier series representation of $\Phi_R$, and determined the RAO again by least-squares fitting (Section 7).

3.  A final approach focused on low-dimensional properties of the RAO (see Section 8).

# 6   Ansatz-free solutions after data selection

In this approach the idea is to solve equation (3) for fixed frequency $\omega$ and then repeat for all 64 frequencies for which there are both respons and wave data available. For fixed $\omega$ the equation reads:

$$S_R = \Phi_R(\theta_1)S_\zeta(\theta_1) + \Phi_R(\theta_2)S_\zeta(\theta_2) + \ldots + \Phi_R(\theta_{90})S_\zeta(\theta_{90});$$

where $\Phi_R(\theta_1), \Phi_R(\theta_2), \ldots, \Phi_R(\theta_{90})$ are 90 unknowns.[1] Thus if one obtains 90 of these equations, then, generically, it should be possible to solve for the unknowns. From every simultaneous measurement of $S_R$ and $S_\zeta$ it is possible to obtain such an equation.

## 6.1   Data selection

In real life some of the data are bad. For instance, when a ship passes the measuring buoy, this affects $S_\zeta$, but does not change $S_R$. The relationship resulting from this measurement will be inherently false. To reduce the impact of erroneous data we make a selection, by taking at given frequency $\omega$ the data with the highest response $S_R$ at that frequency. The idea is that, to obtain a good relation at a given frequency, the frequency should be represented in the measurement. This is guaranteed if the FPSO shows a response at this frequency.

Is, for fixed frequency, every angle represented in some of the chosen data? If $S_\zeta(\omega, \theta)$ is small in every measurement, then the response of the ship to components of waves coming from this angle is impossible to determine. As a consequence the RAO may have a peak at this angle, without any meaning. This corresponds to the RAO being (partly) underdetermined. This has not been checked during the Study Group.

---

[1]Since both 0 and 360 degrees are represented in the data, it has been decided to exclude the data for 360 degrees from the calculations in this approach.
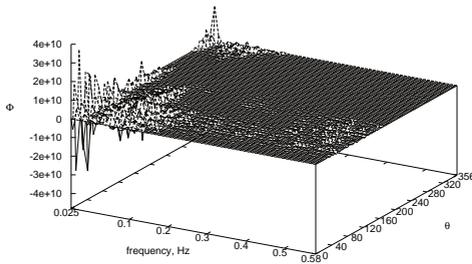
Figure 2: RAO calculated from data with 100 highest stress responses.



Figure 1: unconstrained RAO with negative components.
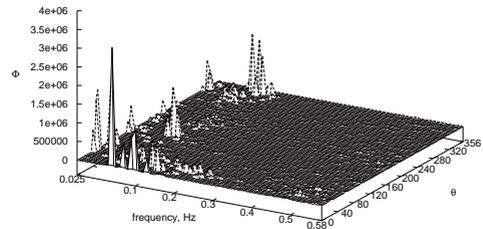


Figure 3: RAO calculated from data with 200 highest stress responses.

## 6.2 Least-squares solutions

Use of the unconstrained least squares solver (the MATLAB backslash operator) leads to a solution with negative components. This is illustrated by Figure 1, where the RAO computed from 100 data points with the highest stress response is plotted. Along the vertical axes the component of the RAO $\Phi_R(\omega, \theta)$ is drawn for each of the 90 angles $\theta$ and each of the 64 frequencies $\omega$. Since the RAO should be non-negative, the unconstrained solver is not useful.

Thus we switched to the constrained least-squares `lsqnonneg` solver, since this solver finds a least squares solution under the constraint that every component must be non-negative. In figures 2 and 3, results are shown that are computed using respectively the 100 and 200 data with the highest stress response, for every frequency separately. As one can see, the solutions are very

spiky. Moreover, it has been observed that these spikes have the tendency to move to a neighbouring angle upon small changes in the input data.
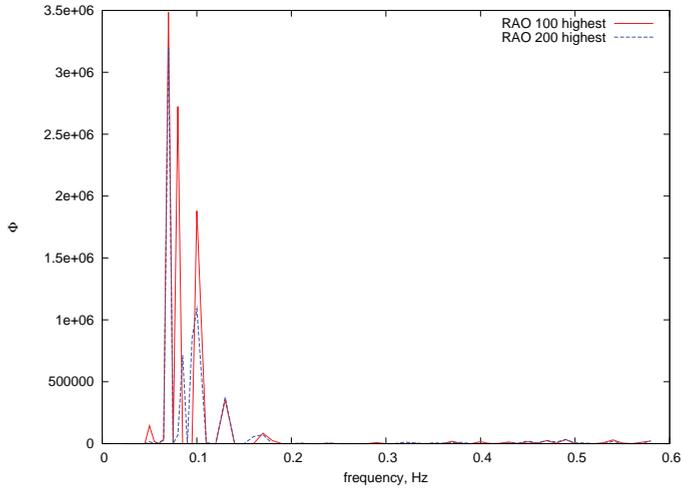


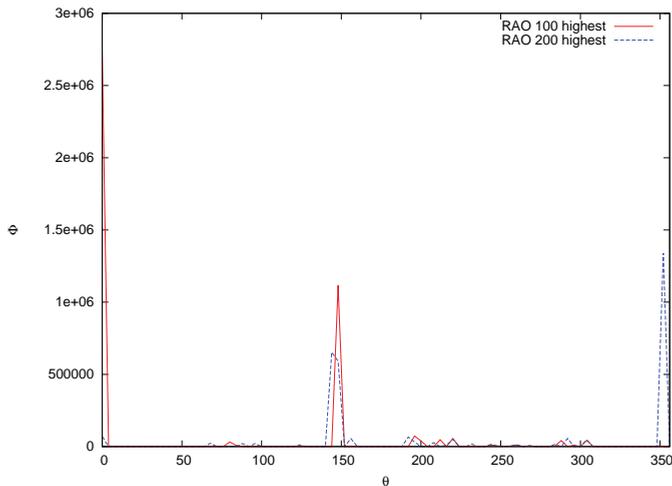Figure 4: Graph of $\Phi_R(\omega)|_{\theta=0}$.



Figure 5: Graph of $\Phi_R(\theta)|_{\omega=0.8}$.

If we fix $\theta = 0$, then Figure 4 shows graphs of $\Phi_R$ as a function of $\omega$, which corresponds to taking a slice from Figures 2 and 3. The peak of the solid red line at $\omega = 0.8$ is not present in the dashed blue line. If we fix $\omega = 0.8$, then Figure 5 shows graphs of $\Phi_R$ as a function of $\theta$, which corresponds to taking a

slice in the other direction. From this graph we see that for the 'dashed blue' RAO based on 200 data, there is a peak for $\omega = 0.8$ near $\theta = 0$, at $\theta = 352$. This is illustrated further by the behaviour near $\theta = 150$. Although in Figure 5 the RAOs practically coincide near $\theta = 150$, this will not be reflected by taking slices for fixed $\theta = 144$ or $\theta = 148$.

## 6.3 Intermediate conclusion

The calculations shown in this section suggest that using the least-squares method one can calculate an approximate RAO, but the resulting RAO will be rather sensitive to differences in data point selection. Because the computed RAOs contain spikes instead of having a more smooth profile, it is not possible to reliably plot $\Phi_R(\omega)$ for a fixed $\theta$.

# 7   Fourier expansions

## 7.1   Motivation

In the previous section we showed that, most likely, the straightforward least-squares approach leads to a sensitive dependence of the RAO on the choice of the data. This is a common occurrence when dealing with inverse problems, and is intimately related to the intrinsic ill-posedness of the problem (see again e.g. [6]). We now investigate whether this issue can be limited by restricting the set of RAO's to a smaller set.

   We postulate a solution $\Phi_R$ of the form

$$\Phi_R(\omega, \theta) = K(\omega)\Psi(\theta). \tag{6}$$

Such an expression allows to consider dependency on $\omega$ and $\theta$ separately, and simplifies our calculations. For more precise approximation it is also worthwhile to replace (6) by

$$\Phi_R(\omega, \theta) = \sum_{\ell=0}^{n_\ell} K_\ell(\omega)\Psi_\ell(\theta). \tag{7}$$

Due to the anisotropy of the ship's geometry it was suggested by MARIN to choose $\Psi_\ell(\theta) = \cos(\ell\theta)$. Thus the final form of our approximation Ansatz is

$$\Phi_R(\omega, \theta) = \sum_{\ell=0}^{n_\ell} K_\ell(\omega)\cos(\ell\theta). \tag{8}$$

This Ansatz can be viewed as representing $\Phi_R$ by a truncated Fourier series in the terms of $\theta$ variable.

   This approach again defines a linear least squares problem, which we refer to as the LLSP. As a result we expect to find $K_\ell(\omega)$ which determine the final

approximation of the solution. We will estimate residuals for different numbers of terms $n_\ell$ in (8). Moreover the relative error of the solution $\Phi_R(\omega, \theta)$ and $S_R(\omega)$ predicted by our model will be estimated in section 7.4 for different amounts of data used.

## 7.2   Implementation of the model

For each fixed $\omega$ we define

$$
P := \begin{pmatrix} S_\zeta^{(1)}(\omega, \theta_1) & \dots & S_\zeta^{(N)}(\omega, \theta_1) \\ \dots & \dots & \dots \\ S_\zeta^{(1)}(\omega, \theta_{91}) & \dots & S_\zeta^{(N)}(\omega, \theta_{91}) \end{pmatrix}, \tag{9}
$$

and

$$
C := \begin{pmatrix} 1 & \cos\theta_1 & \dots & \cos n_\ell\theta_1 \\ 1 & \cos\theta_2 & \dots & \cos n_\ell\theta_2 \\ \vdots & & & \vdots \\ 1 & \cos\theta_{91} & \dots & \cos n_\ell\theta_{91} \end{pmatrix}. \tag{10}
$$

The LLSP then consists of solving, in the least-squares manner, the equation $Ax = b$, with

$$
A = P^T C, \qquad b = [S_R^{(1)}(\omega), \dots, S_R^{(N)}(\omega)]^T, \tag{11}
$$
$$
\text{and} \quad x = [K_1(\omega), \dots, K_{n_\ell}(\omega)]^T.
$$

By repeating the procedure for each $\omega$ we obtain $K_\ell$ and thus $\Phi_R(\omega, \theta)$.

## 7.3   Analysis of the method

It is important to understand how well this model constructs $\Phi_R$ and predicts $S_R$. On the other hand, we wish to analyze to which extent the constructed $\Phi_R$ is data-dependent.

## 7.4   Approximation error

First we analyze the approximation error, which is the discrepancy between the exact values of $S_R$ and their approximation by the LLSP.

We split the total available data for the draft 12.5–13.0 into disjoint groups of different sizes. We fix a number $N$ of data points. Let $D_\kappa$, $\kappa = 1, 2$ be two disjoint sets of data of size $N$. Also let $K^{[\kappa]}$ be the solution of the LLSP with data $D_\kappa$, i.e. the minimizer of the norm of the residuals for data set $D_\kappa$. In other words, we have

$$
K^{[\kappa]}(\omega) := \arg\min_x \| S_R^{[\kappa]}(\omega) - Ax \|_2,
$$

where $S_R^{[\kappa]}(\omega)$ is the $N$-vector of response data corresponding to data set $D_\kappa$ and $A$ is defined in (11).

Then, for each frequency $\omega$, we define the approximation error of LLSP-solution $\kappa$ for the data $D_\lambda$ as follows:

$$F(\omega, K^{[\kappa]}, D_\lambda) := \frac{\|S_R^{[\lambda]}(\omega) - AK^{[\kappa]}(\omega)\|_2}{\|S_R^{[\lambda]}(\omega)\|_2}, \qquad \kappa, \lambda = 1, 2, \qquad (12)$$

where $S_R^{[\kappa]}(\omega)$ is the $N$-vector of response data corresponding to data set $D_\kappa$, and $K^{[\lambda]}$ is the solution of the LLSP for the data set $D_\lambda$.

First we study the influence of the number $N$ of data points. We choose two sets $D_1$ and $D_2$ of size $N = 350$ corresponding to the data from February and August 2008. We compare $F(\omega, K^{[1]}, D_1)$ and $F(\omega, K^{[2]}, D_1)$ for the amount of terms in (8) $n_\ell = 3$. This can be interpreted as a measure of how well data $D_2$ predicts data $D_1$.
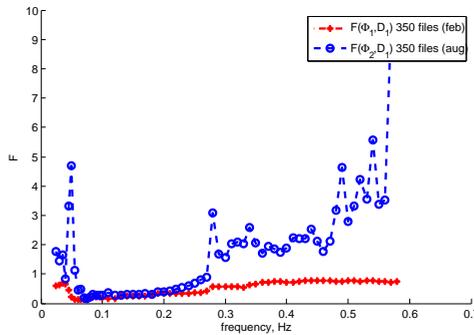


Figure 6: The approximation error for $F(\omega, K^{[1]}, D_1)$ and $F(\omega, K^{[2]}, D_1)$, $N = 350$.

The high value of the $F(\omega, K^{[2]}, D_1)$ in Figure 6 may well be explained by the fact that during different seasons the intensity of some frequencies differs. We next compare $F(\omega, K^{[2]}, D_2)$ and $F(\omega, K^{[1]}, D_2)$. In Figure 7 we see that the prediction of the August response by the February data is much better than vice versa. It can be useful to see how this fact changes with increasing the size of data sets used.

From Figures 8–11 it is clear that the bigger data sets we use, the closer to each other the approximation errors of the corresponding solutions become. But for several small frequencies the approximation error is still very high. We believe that this happens due to measurement errors of the experiments.

At this stage the conclusion is that it is best to use the biggest available amount of data for the further analysis of the approximation error on the number of terms in expansion (8). Now, in Figures 12–15, we vary the number of
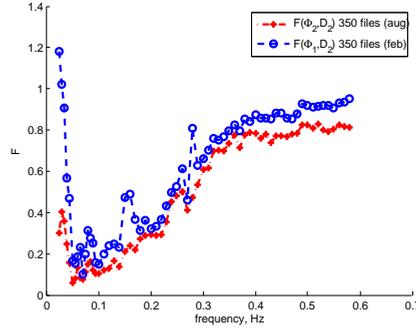
Figure 7: The approximation error for $F(\omega, K^{[2]}, D_2)$ and $F(\omega, K^{[1]}, D_2)$, $N = 350$.
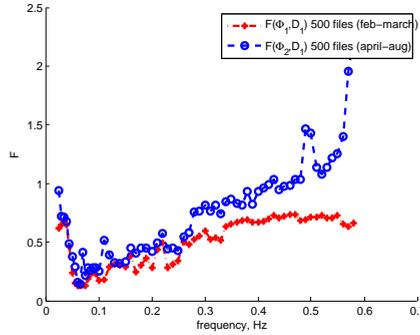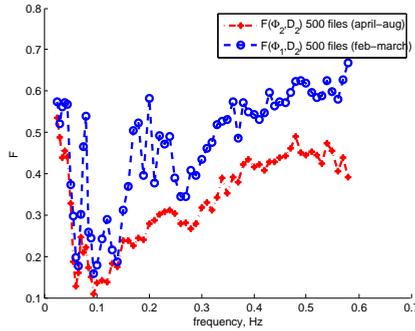


Figure 8: The approximation error for $F(\omega, K^{[1]}, D_1)$ and $F(\omega, K^{[2]}, D_1)$, $N = 500$.

terms $n_\ell$ and fix the size of the data sets $N = 715$, as this is the half of the available data for the chosen draft. The case $n_\ell = 0$ corresponds to the fact that $\Phi_R$ is approximated by a function that is constant in $\theta$.

We study not only the approximation error but also two other values of interest ($\varepsilon(\omega)$ and $\varepsilon(\theta)$ defined in equations (13),(14)). The first of them is the relative error of $\Phi_R^{[\kappa]}$ with respect to $\Phi_R^{[\lambda]}$ for each frequency:

$$\varepsilon(\omega) = \frac{\|\Phi_R^{[\kappa]}(\omega, \cdot) - \Phi_R^{[\lambda]}(\omega, \cdot)\|_2}{\|\Phi_R^{[\kappa]}(\omega, \cdot)\|_2}, \tag{13}$$

where $\Phi_R^{[\kappa]}(\omega, \theta)$ and $\Phi_R^{[\lambda]}(\omega, \theta)$ are approximated values of $\Phi_R$ calculated via corresponding solutions $K^{[\kappa]}$ and $K^{[\lambda]}$ of LLSP using two distinct data sets $D_\kappa$ and $D_\lambda$ of the same size. The norms above are the $L^2$-norms over $\theta$.

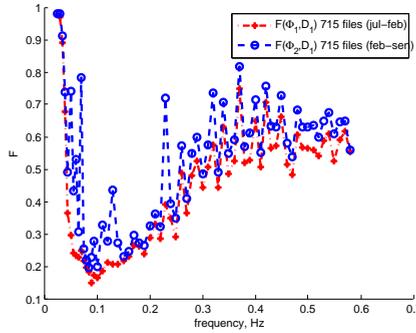Figure 9: The approximation error for $F(\omega, K^{[1]}, D_2)$ and $F(\omega, K^{[2]}, D_2)$, $N =$ 500.



Figure 10: The approximation error for $F(\omega, K^{[1]}, D_1)$ and $F(\omega, K^{[2]}, D_1)$, $N =$ 715.

A similar quantity can be calculated for each angle $\theta$, where the norms are calculated by summing over $\omega$:

$$\varepsilon(\theta) = \frac{\|\Phi_R^{[\kappa]}(\cdot, \theta) - \Phi_R^{[\lambda]}(\cdot, \theta)\|_2}{\|\Phi_R^{[\kappa]}(\cdot, \theta)\|_2}. \tag{14}$$

Increasing $n_\ell$ gives the system more freedom to adjust the parameters. From this point of view using more terms is a good idea. At the same time it leads to an increasing amount of oscillations, as can be seen in Figures 12-15. From the numerical experiments we suggest to use $n_\ell = 2$, because of two reasons:

- the peak of the approximation error for small frequencies is not high yet;

- the relative errors $\varepsilon(\omega)$ and $\varepsilon(\theta)$ are still reasonable (below 1).
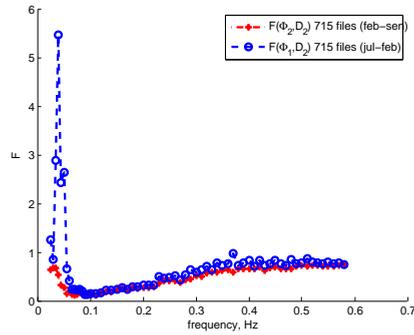
Figure 11: The approximation error for $F(\omega, K^{[1]}, D_2)$ and $F(\omega, K^{[2]}, D_2)$, $N = 715$.
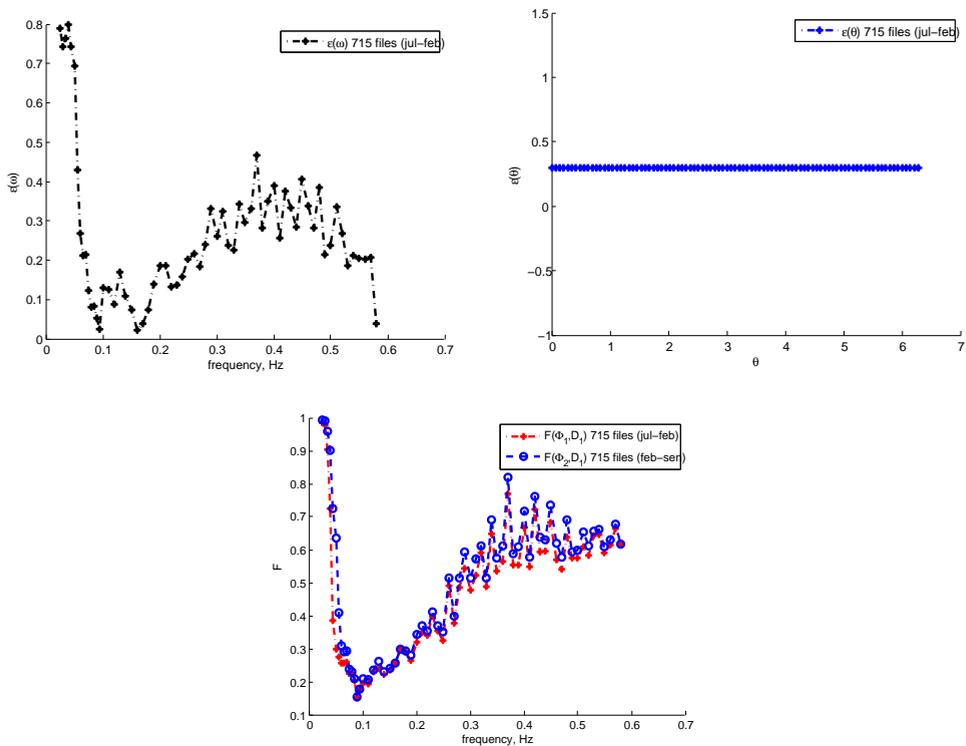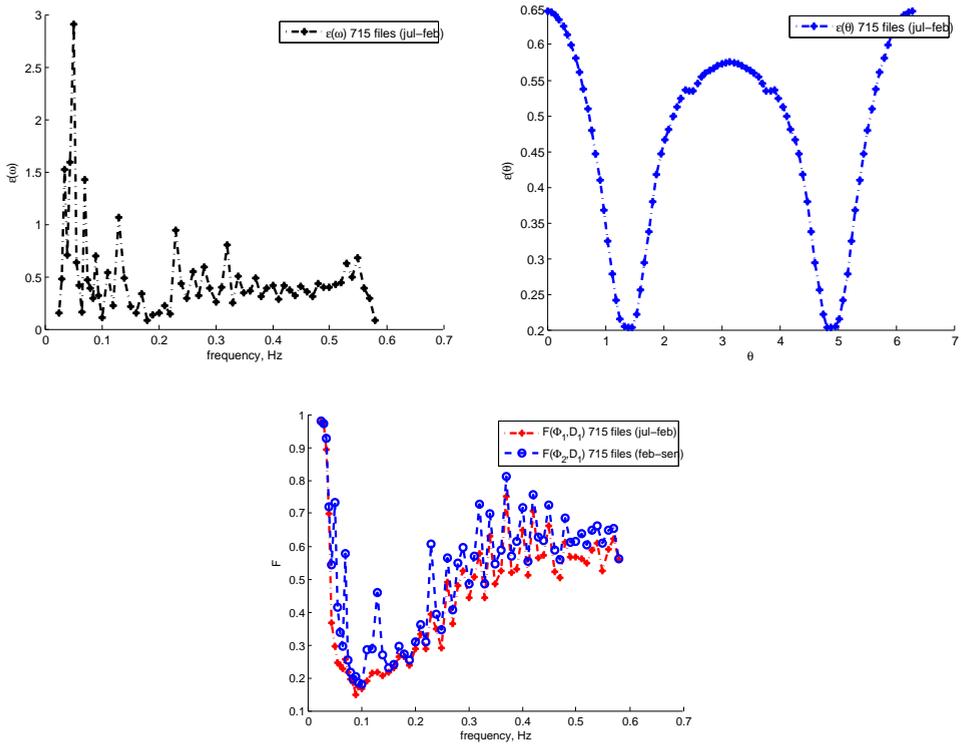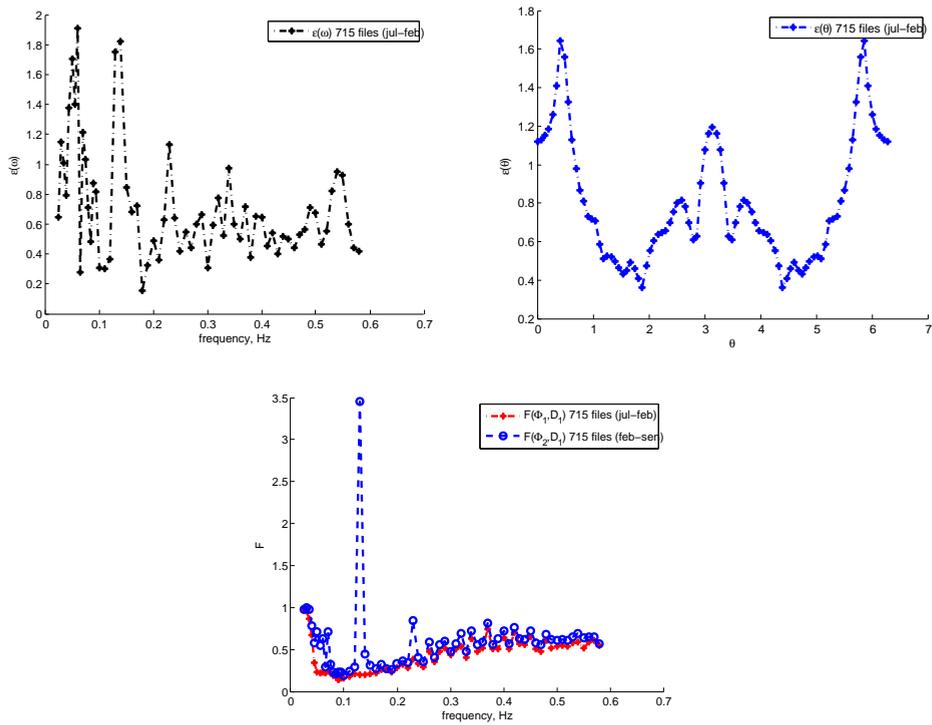


Figure 12: The approximation error for $F(\omega, K^{[1]}, D_1)$ and $F(\omega, K^{[2]}, D_1)$, $n_\ell = 0$. Note that $\varepsilon(\theta)$ is constant, since with $n_\ell = 0$, $\Phi_R$ is independent of $\theta$.

Figure 13: The approximation error for $F(\omega, K^{[1]}, D_1)$ and $F(\omega, K^{[2]}, D_1)$, $n_\ell = 2$.

Figure 14: The approximation error for $F(\omega, K^{[1]}, D_1)$ and $F(\omega, K^{[2]}, D_1)$, $n_\ell = 6$.
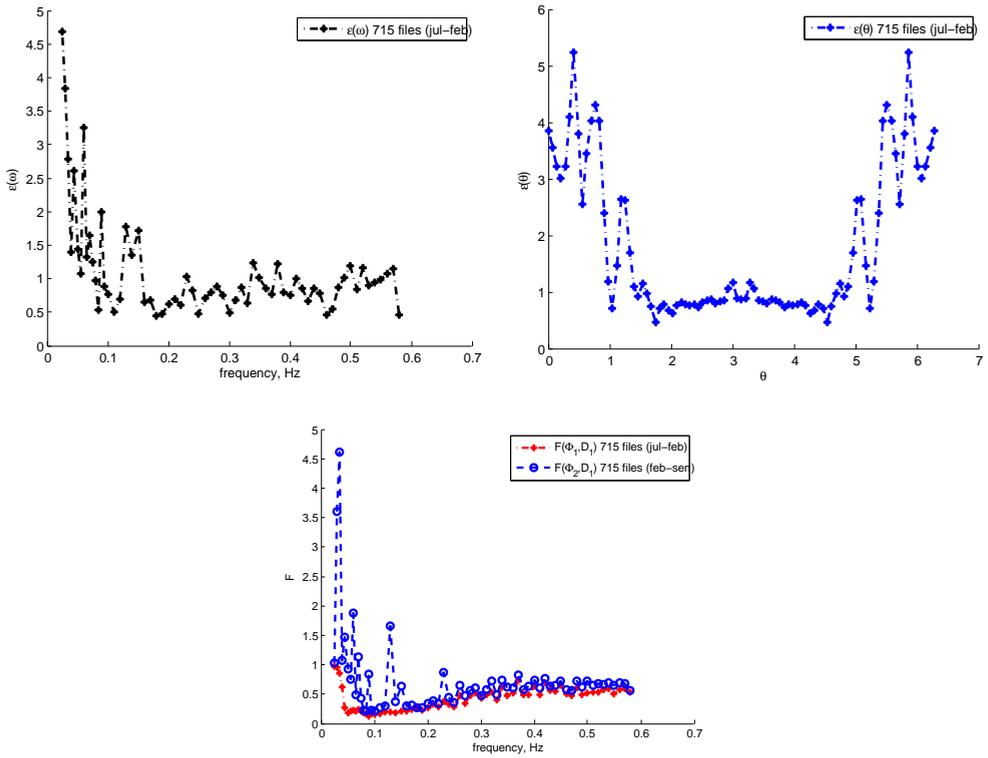
Figure 15: The approximation error for $F(\omega, K^{[1]}, D_1)$ and $F(\omega, K^{[2]}, D_1)$, $n_\ell = 10$.

## 7.5   Prediction of $S_R$

The comparison of predicted (dashed line) and experimental dependence (solid line) of $\Phi_R$ on $\omega$ is done for different data files. We again use the set of 715 files and predict the values of $S_R$ for three specific data points which are not included in those 715 files. All calculations are done for $n_l = 2$. Also corresponding $\Phi_R(\omega)$ for several angles is presented in Figures 19-21.
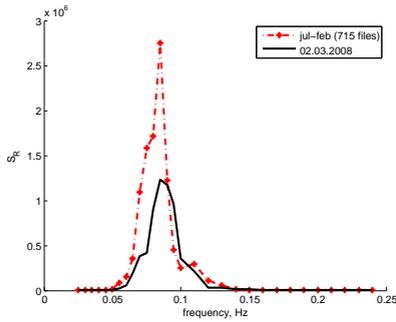


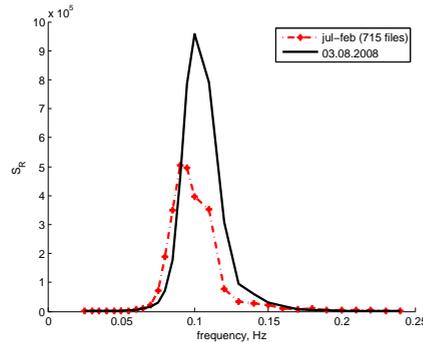Figure 16: The predicted values have an overshoot.



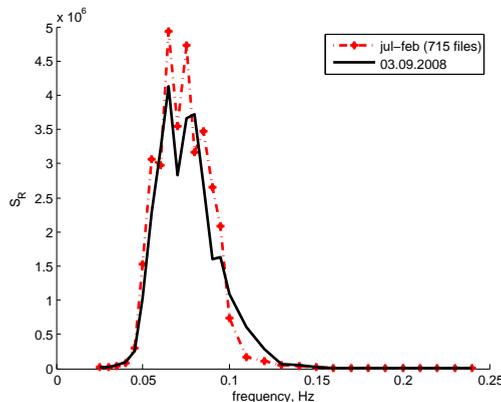Figure 17: The predicted values are too small.



Figure 18: The predicted and experimental behavior fit well together.

Figures 16–18 show that, depending on the date which we pick for forecast, the result differs. One way of explaining this phenomenon is due to experimental errors. Results obtained for the 1st and 2nd of July 2008 on Figures 22 and
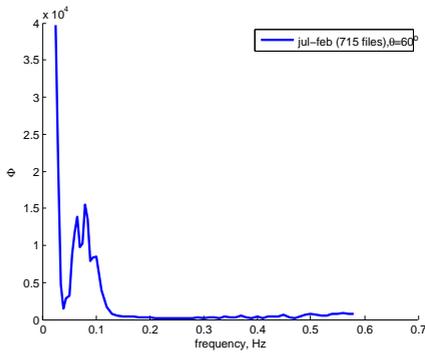
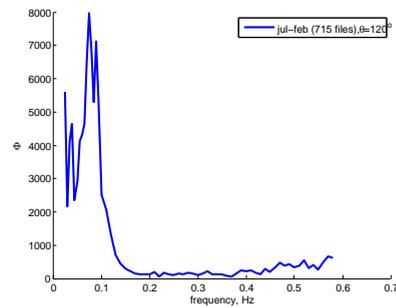Figure 19: The prediction of $\Phi_R(\omega, 60)$.
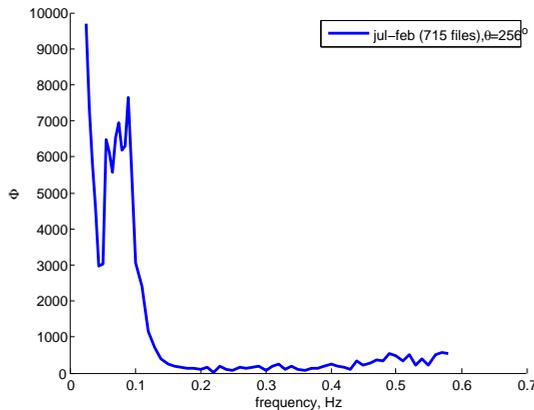


Figure 20: The prediction of $\Phi_R(\omega, 120)$.



Figure 21: The prediction of $\Phi_R(\omega, 256)$.

23 are examples of this. Usually the response on consequent days changes continuously but for these dates it is not the case.

Another reason could be an insufficient period of measurements used in calculations. Therefore our recommendation is to use the observations of several years to predict $\Phi_R$.

## 7.6   Intermediate conclusions

From these calculations we draw the following conclusions:

   1. If the number of data points is large enough ($N \geq 500$ seems a reasonable
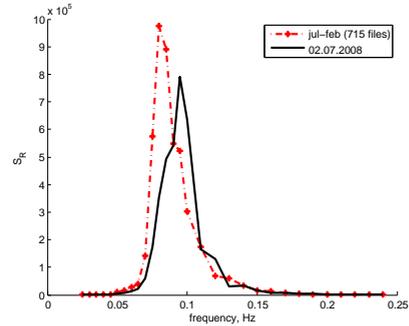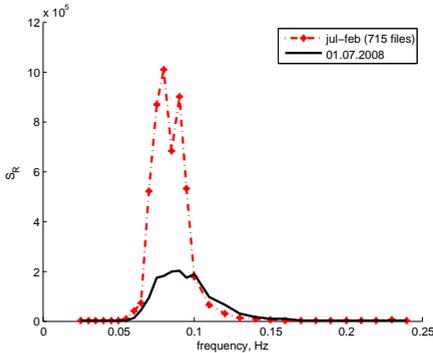
Figure 22: Results for the 1st of July.   Figure 23: Results for the 2nd of July.

lower bound) then the cross-approximation error $F(\omega, K^{[2]}, D_1)$ often is practically as good as the self-approximation error $F(\omega, K^{[1]}, D_1)$. In words: the least-squares error for data 1, based on the parameters determined with data 2, is close to the error calculated with the optimal parameters for data 1. (See e.g. Figures 12–15).

2. The number $n_\ell$ of Fourier modes is a free parameter in this inverse problem. By definition, the self-approximation error decreases with increasing $n_\ell$, since the minimization is performed over larger sets. But for larger $n_\ell$, the Fourier coefficients $K_\ell$ becomes highly sensitive to the choice of data. The calculations done above suggest to keep $n_\ell$ low, e.g. $n_\ell \approx 2$.

# 8   Reduced measures

During the Study Group the question arose whether the identification of the RAO might be used to *detect* fatigue: can fatigue cracks determine a modified stress response, and therefore result in a modified RAO? By tracking changes in the RAO over time, we thought that these changes might be detected. This idea turned out to be incorrect. Indeed a fatigue crack cannot determine any significant change in the vertical bending moment, by which the global behavior of the structure is analyzed. This consideration has been communicated to us by MARIN.

In the spirit of the the previous section, we focus here on a particular Ansatz, investigating whether an RAO could be determined with sufficient accuracy and confidence. The ill-posed nature of the problem suggests to replace the aim of determining $\Phi_R$ by determining some low-dimensional properties of $\Phi_R$ that might (a) function as fatigue markers, and (b) be more stable.

Given that our data only spans 15 months, and that the fatigue time scale is expected to be longer than this, it was difficult to test any hypothesis concerning stability with respect to time. Instead, we investigate below a simple hypothesis concerning a special form of RAO with respect to the dependence on $\theta$ and $\omega$.

Equation (3) can be written as

$$\forall \omega, k : \quad \sum_{\theta} \Phi_R(\omega, \theta) S^{(k)}(\omega, \theta) = 1, \tag{15}$$

where $S^{(k)}(\omega, \theta) := S_\zeta^{(k)}(\omega, \theta)/S_R^{(k)}(\omega)$. One Ansatz for $\Phi_R$ would be that $\Phi_R$ is of the form

$$\Phi_R(\omega, \theta) = c(\theta)(S^{(k)})^{-1}(\omega, \theta), \tag{16}$$

for some function $c(\theta)$ satisfying $\sum_{\theta} c(\theta) = 1$. Note that since $\Phi_R$ is $k$-independent, this requires $S^{(k)}$ also to be $k$-independent. This is a condition that we can test directly the available experimental data.

## 8.1 Data analysis

We analyse if the ratio $(S^{(k)})^{-1}$ is data- ($k$-) independent. This analysis is achieved by means of an estimator. We average the ratio among measurements, but they must belong to the same draft to avoid the draft dependence (that will be analysed in the following). So we define

$$f_d(\omega, \theta) := \frac{1}{\tilde{S}(\omega, \theta, d)} = \frac{\sum_{k \in I(d)} S_k^{-1}(\omega, \theta, d)}{\#I(d)}, \tag{17}$$

where $I(d)$ is the set of all the measurements obtained for a certain draft. From now on for brevity we write $S_k^{-1}$ instead of $(S^{(k)})^{-1}$. If there is an independence; then we expect the standard deviation to be small. We analyse then the relative error:

$$g_d(\omega, \theta) = \sigma^2 = \frac{\sum_{k \in I} (S_k^{-1} - \tilde{S}^{-1})^2}{\#I}, \tag{18}$$

$$\text{relative error} := h_d(\omega, \theta) = \frac{\sqrt{g(\omega, \theta)}}{f(\omega, \theta)}. \tag{19}$$

A suitable way to analyse the relative error is to perform the average of the relative error over angles or frequencies:

$$a(\omega) := \frac{\sum_{\theta} h(\omega, \theta)}{\#\theta}, \quad b(\theta) := \frac{\sum_{\omega} h(\omega, \theta)}{\#\omega}. \tag{20}$$

The above formulas give us an estimator of the oscillations occurring in the data, depending only on one variable. We perform this procedure because we cannot represent all the values of $h(\omega, \theta)$ (it is a $90 * 64$ matrix). The problem that can appear when averaging is related to huge oscillations giving an irrelevant average. This will not be our case as it will be showed in the following.

## 8.2   Draft dependence

We need to make a reasonable choice of a single draft. To do this we analyze the total average of the relative error to check to which extent the independence (of the ratio with respect to data) is a reasonable assumption and to see which measurements present a strong correlation:

$$c(d) := \frac{\sum_\theta \sum_\omega h(\omega, \theta, d)}{\#\omega \times \#\theta} = \frac{\sum_\theta b(\theta, d)}{\#\theta} = \frac{\sum_\omega a(\omega, d)}{\#\omega}. \tag{21}$$

Table 2 shows the value of $c(d)$ for each $d$. Note that the values for the middle

| $c(d)$ | 142% | 12.1% | 3.8% | 2.2% | 1.7% | 2.7% |
|--------|------|-------|------|------|------|------|
| Draft  | 9.5  | 10    | 10.5 | 11   | 11.5 | 12   |
| $c(d)$ | 2.2% | 2%    | 2%   | 2.4% | 7.1% | 9.5% |
| Draft  | 12.5 | 13    | 13.5 | 14   | 14.5 | 15   |

Table 2: For each draft $d$ the value of $c(d)$ estimates to which extent the function $S_k^{-1}$ can be considered measurement- ($k$-) independent.

range of $d$ are relatively small, giving support to the conjecture (16). In choosing a specific draft $d$ for further analysis, it makes sense to avoid the extremal values for which $c(d)$ is larger.

## 8.3   Correlation

In Figure 8.3, we plot the functions $a(\omega)$, $b(\theta)$ defined in (20). They refer to the fixed draft 12–12.5 m, that presents a low total average ($c(d)$). We note that the values are relatively small and they show weak fluctuations. This gives more relevance to the choice of the estimator $c(d)$ and it is a way to quantify the independence of the ratio $S_k^{-1}$ with respect to measurements.

## 8.4   Time evolution

The small values of $c(d)$ allow us to focus in the data analysis on a single draft. We now want to investigate whether the time scale of the data measurements could provide a reasonable RAO. A necessary condition is that the vessel does not experience excessive changes in its structure. In order to check this fact, we choose suitable estimators and we analyze their values on each month in a time range of 15 months. For fixed $\theta$, we consider $N_{\exp}$ measurements in a certain time range. We use (a normalized) $S^{-1}$ as a probability distribution, then, and we compute its $\omega$-average for each $\theta$:

$$\omega_\theta^{(k)} = \frac{\sum_\omega \omega S^{-1}(\omega, \theta)}{\sum_\omega S^{-1}(\omega, \theta)}, \qquad k = 1, \ldots, N_{\exp}. \tag{22}$$
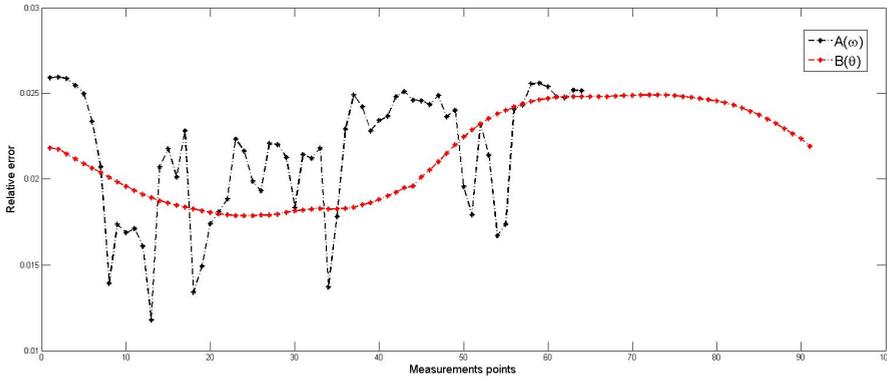
Figure 24: Relative standard deviations.

Now we average along measurements and determine the mean value and standard deviation at fixed angles:

$$\bar{\omega}_\theta := \frac{1}{N_{\exp}} \sum_{k=1}^{N_{\exp}} \omega_\theta^{(k)}, \tag{23}$$

$$\sigma_\theta^2 := \frac{1}{N_{\exp}} \sum (\bar{\omega}_\theta - \omega_\theta^{(k)})^2, \tag{24}$$

where $\omega_\theta^{(k)}$ is given by (22). $\bar{\omega}_\theta$ can be interpreted as an average eigenfrequency of the structure.

In Table 3 are shown average and standard deviations related to five angles, in a time range of 15 months. We note that the values at 0 and 360 coincide,

| $\theta$ | 0 | 90 | 180 | 270 | 360 |
|---|---|---|---|---|---|
| $\bar{\omega}_\theta$ | 0.1337 | 0.1359 | 0.1396 | 0.1704 | 0.1337 |
| $\sigma_\theta$ | 0.0255 | 0.0331 | 0.0426 | 0.0516 | 0.0264 |

Table 3: Angles, averages and standard deviations.

confirming the expected periodicity in $\theta$ of the data sets.

In Figure 25 we plot the average and standard deviations for each month, i.e. $\bar{\omega}_\theta$ and $\sigma_\theta^2$ calculated for each month separately. We choose two angles, $\theta = 90$ and $\theta = 270$. The number of measurements per month is given by the following table:

| 1st | 2nd | 5th | 8th | 9th | 10th | 12th | 13th | 14th | 15th |
|-----|-----|-----|-----|-----|------|------|------|------|------|
| 106 | 59  | 140 | 473 | 37  | 78   | 11   | 109  | 351  | 117  |

Table 4: Measurements analyzed per months, starting from July 2007, ending in September 2008.
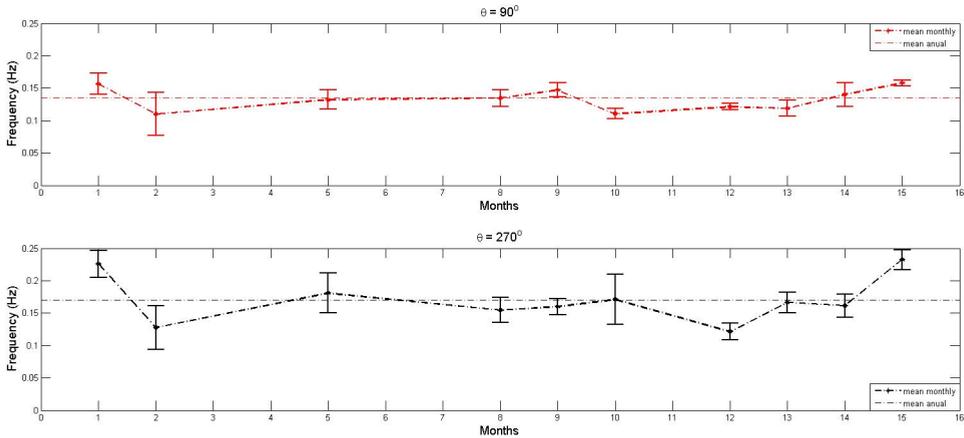


Figure 25: Monthly averages $\bar{\omega}_\theta$ and standard deviations $\sigma_\theta$ for two angles $\theta = 90, 270$.

## 8.5   Intermediate conclusions

Figure 25 shows no significant drift of $\omega_\theta$ over the five months, and the fluctuations are of the magnitude that is to be expected. This observation can be interpreted as suggesting that the object that we calculate here (the expected frequency, according to the weighting given by the 'probability distribution' $S^{-1}$) is approximately constant over the 15 months of the data. This consideration together with Table 2 estimates to which extent (16) is a reasonable choice.

An interesting analysis would be to have a $\theta$-dependent picture of the behavior of the structure measured by the fluctuations of the monthly averages and their relative standard deviation, which, during SWI 2012, we thought to be more considerable in those directions where the vessel is affected by more relevant damage and structural changes. This idea turned out to be wrong, after discussing with our collaborator from MARIN, as we already mentioned at the beginning of this section.

# 9 Summary and conclusions

We have seen that despite the large amount of data, determining the RAO to any accuracy is a hard problem. This is illustrated, for instance, in the strong data-dependence that we observed when doing direct (constrained) least-squares fitting in Section 6. This is a classical difficulty in inverse problems, and is related to the ill-posed nature of the problem.

The classical 'solution' to this difficulty is to restrict the class of admissible RAOs and perform the fitting in this smaller class. This is the core idea in Section 7 and Section 8 (see respectively equations (6) and (16)), where a special form for RAO has been postulated. This restriction brings in Section 7 the identification of an RAO.

A different form of RAO has been considered in Section 8, where initially we tried to address the question whether the data could provide information about existence of fatigue-induced drift. The performed data analysis is meant to verify to which extent (confidence) the Ansatz (16) is a reasonable guess, as a preliminary step in the identification of an RAO.

There are many possible avenues for further research and algorithm construction. Below we sum up those that we considered during the five-day SWI 2012 study group to be the most important.

- All methods should be set in a suitable stochastic framework in order to treat the unavoidable *noise* brought in by the measurements. We expect a faithful modelling of the characteristics of this noise will improve the quality of the fitting methods.

- Connected to the above consideration is the study of the *rank* of the available data files. Referring for simplicity to the Ansatz-free approach, it would worth analyzing how *independent* the data are, in order to yield the solvability of the linear system of equations. Intuitively, this is related to the non-vanishing determinants of the sub-matrices associated to the linear system.

## Acknowledgments

# References

[1] J. Journée and W. Massie, *Offshore Hydromechanics.* Delft University of Technology, Course notes;
http://www.shipmotions.nl/DUT/LectureNotes/OffshoreHydromechanics.pdf

[2] E. H. Cramer, R. Løseth and K. Olaisen  Fatigue assessment of ship structures. *Marine Structures*,8:359–383, 1995.

[3] I. Drummen, M.K. Wu, M. L. Kaminski, and T. Moan, Numerical investigation into the application of response conditioned waves for long-term nonlinear fatigue analyses of rigid hulls. *Ocean Engineering*, 36:1208–1216, 2009.

[4] I. Drummen, G. Storhaug, and T. Moan, Experimental and numerical investigation of fatigue damage due to wave-induced vibrations in a containership in head seas. J. Mar. Sci. Tech., 13:428–445, 2008.

[5] B. Girod, R. Rabenstein, and A. Stenger, *Signals and Systems.* Wiley, NY, 2001.

[6] A. Kirsch, *An Introduction to the Mathematical Theory of Inverse Problems*, Springer Verlag, 2011.

[7] A. Powell, *An Introduction to Acoustic Fatigue.* in Acoustical Fatigue in Aerospace Structures, NY, 1965.

[8] A. Tarantola, *Inverse Problem Theory and Methods for Model Parameter Estimation.* SIAM, NY, 2005.